2540–2553 *Nucleic Acids Research, 2012, Vol. 40, No. 6* *Published online 29 November 2011*
doi:10.1093/nar/gkr1140

Analysis of the RNA chaperoning activity of the hepatitis C virus core protein on the conserved 3′X region of the viral genome

Kamal Kant Sharma[1], Hugues de Rocquigny[1], Jean Luc Darlix[1], Jean-Pierre Lavergne[2], François Pénin[2], Jean-Marc Lessinger[1] and Yves Mély[1,*]

[1]Laboratorie de Biophotonique et Pharmacologie, UMR 7213 CNRS, Faculté de Pharmacie, Université de Strasbourg, 74, Route du Rhin, 67401 Illkirch, Cedex and [2]Institut de biologie et Chimie des Protéines, Bases Moléculaires et Structurales des Systèmes infectieux, UMR 5086 CNRS, Université de Lyon, 7 Passage du Vercors, 69367 Lyon, France

Received October 7, 2011; Revised November 5, 2011; Accepted November 9, 2011

ABSTRACT

The core protein of hepatitis c virus (HCV) is a structural protein with potent RNA chaperoning activities mediated by its hydrophilic N-terminal domain D1, which is thought to play a key role in HCV replication. To further characterize the core chaperoning properties, we studied the interactions between core D1 and the conserved HCV 3′X genomic region required for genome replication. To this end, we monitored the real-time annealing kinetics of native and mutated fluorescently labelled 16-nt palindromic sequence (DLS) and 27-nt Stem Loop II (SL2) from X with their respective complementary sequences. Core D1 and peptides consisting of the core basic domains were found to promote both annealing reactions and partly switch the loop–loop interaction pathway, which predominates in the absence of peptide, towards a pathway involving the stem termini. The chaperone properties of the core D1 peptides were found to be mediated through interaction of their basic clusters with the oligonucleotide phosphate groups, in line with the absence of high affinity site for core on HCV genomic RNA. The core ability to facilitate the interconversion between different RNA structures may explain how this protein regulates RNA structural transitions during HCV replication.

INTRODUCTION

Hepatitis C virus (HCV) is a major cause of chronic hepatitis, liver cirrhosis and hepatocellular carcinoma (1). Current standard therapy, pegylated interferon-α (PEG-IFN-α) combined with ribavirin, results in a sustained virologic response in ∼50% of patients (2). The HCV genome is a single stranded RNA of ∼9.6 kb length with positive polarity (3), which includes a long open reading frame (ORF) flanked by 5′ and 3′ untranslated, highly conserved and structured regions, named 5′-UTR and 3′-UTR. The 5′-UTR contains an internal ribosome entry site (IRES) which directs cap-independent translation of the ORF. After binding of HCV particles to a complex set of entry factors and internalization into the host cell, the viral RNA genome is released in the cytosol and its IRES binds to ribosomes, allowing the translation of HCV polyprotein at the level of the endoplasmic reticulum membrane. This polyprotein is further processed by cellular and viral proteases to yield the mature structural (core protein, E1 and E2) and non-structural proteins (p7, NS2, NS3, NS4A, NS4B, NS5A and NS5B) ensuring RNA replication and packaging, as well as virion assembly and release from the host cell (4–6).

The genomic RNA plays complex, temporally and spatially regulated roles throughout the virus life cycle, by serving both as a template for minus-strand RNA synthesis and as an mRNA directing the translation of the viral polyprotein and lastly, by being packaged into newly made progeny virions. The UTR sequences contain *cis*-acting elements that are crucial for RNA replication and translation (7–9). The 5′-UTR (341 nt) folds into a four-domain structure that contains in addition to the IRES, upstream signals required for viral RNA synthesis (10,11). The 3′-UTR (230 nt) contains three structurally distinct domains: (i) an upstream variable sequence with VSL1 and VSL2 stem–loops, (ii) a poly (U/UC) tract and (iii) a highly conserved, 98-nt long 3′X-tail, that forms three stem–loop structures (designated as SL1, SL2 and SL3) (12,13) (Figure 1A). Both the X region and a minimal poly(U/UC) tract of ∼40 nt are essential for

*To whom correspondence should be addressed. Tel: +33 03 68 85 42 63; Fax: +33 03 68 85 43 12; Email: yves.mely@unistra.fr

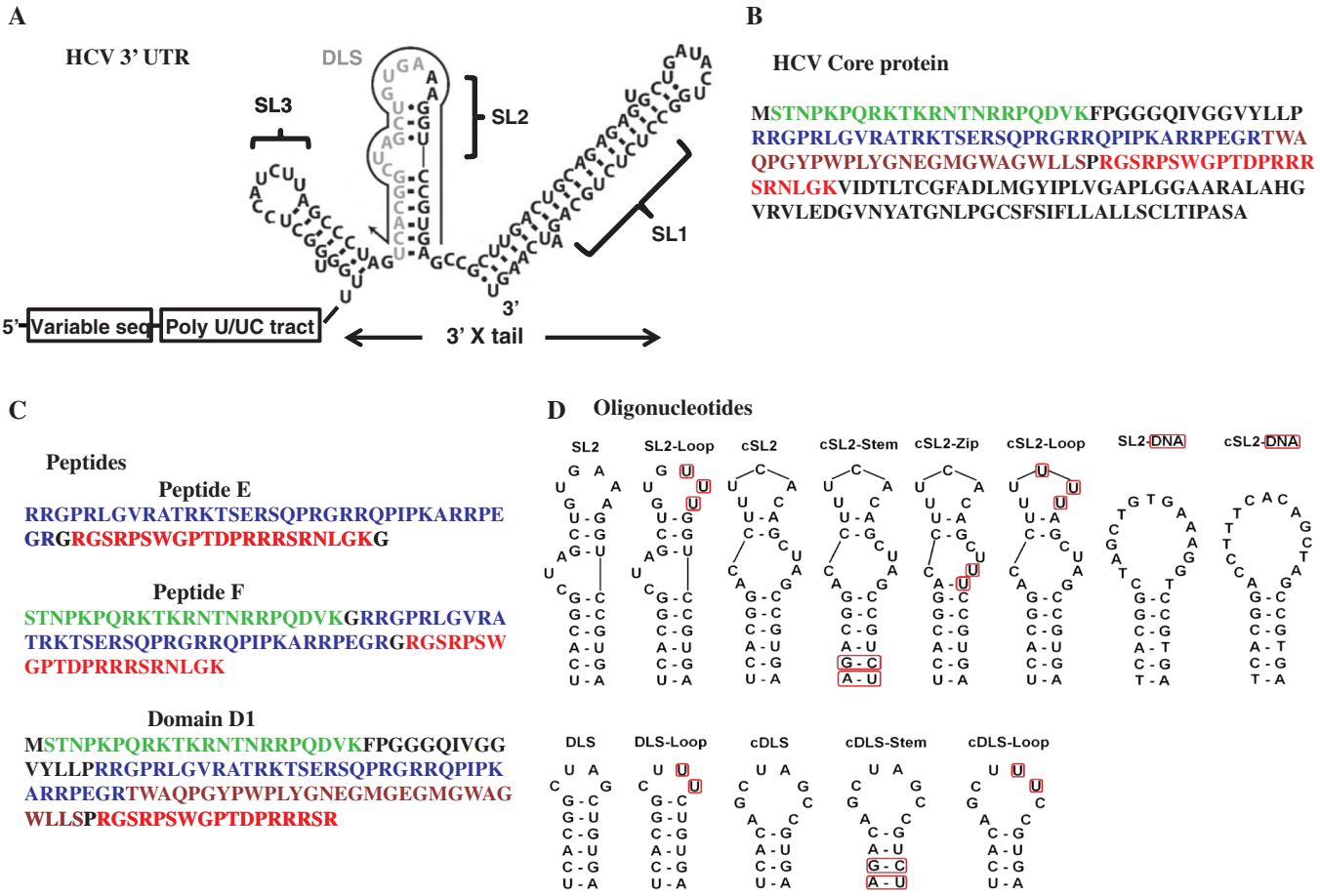

Figure 1. Structure of HCV 3′-UTR (**A**), HCV core protein (**B**) and peptides (**C**) and oligonucleotides (**D**) used in this study. (A) The 3′-UTR contains the variable region, the U-rich region and the 98-nt X tail sequence. The putative dimerization domain (DLS) is in grey [adapted from (26)]. (B and C) The ~117 amino acid long N-terminal D1 domain of the core protein comprises three regions rich in basic residues [BD1 (green), BD2 (blue) and BD3 (red)] and a tryptophan rich domain (brown) while the ~52-amino acid long C-terminal D2 domain is hydrophobic and binds to membranes of the endoplasmic reticulum and lipid droplets. (D) The oligonucleotide sequences are from the 3′X of the HCV genome and their secondary structures were predicted using the mfold program (http://mfold.rna.albany.edu/?q=mfold). The substituted positions in the mutants are boxed in red.

RNA replication (14–18), while the variable region plays some role in RNA replication and *in vivo* infectivity (14–18). The 3′X region is also thought to facilitate the translation of the viral RNA, via the IRES (8). Two alternate conformations are predicted for the 3′X region (19) that includes a sequence of 55 nt, which is fully conserved among HCV strains (20). In addition, this sequence contains a 16-nt long palindrome (DLS), found to be responsible for the dimerization of the HCV RNA *in vitro* (19,20).

The HCV core (Figure 1B) is a basic and dimeric protein thought to oligomerize upon packaging of the genomic RNA (21–23), in order to form the viral nucleocapsid. The mature core protein is constituted by two domains: (i) a N-terminal RNA binding domain D1 of 117 amino acids including three highly basic clusters [BD1–BD3] and (ii) a hydrophobic C-terminal domain D2 mediating the association of core with endoplasmic reticulum membranes and lipid droplets (24,25). The three basic amino acid clusters (BD1–BD3) of the D1 domain are responsible for the nucleic acid chaperone activity (19,26,27) of the HCV core protein. By analogy to other RNA chaperone proteins (28–33), the core protein facilitates the correct folding of RNA molecules by preventing their misfolding or by resolving misfolded RNA structures (34,35). Through its chaperone properties, the core and peptides consisting of the three core basic domains (Figure 1C, peptide F) or only two of them (Figure 1C, peptide E) were shown to promote the annealing of complementary sequences (27), strand exchanges as well as the dimerization of the 3′-UTR sequence of the HCV genome (19,26).

Here, we further characterized the RNA chaperone properties of the core protein by investigating the annealing mechanism of the 16-nt palindromic sequence (Figure 1D, DLS) and the 27-nt Stem Loop II (Figure 1D, SL2) with their complementary sequences, corresponding to the negative strand viral RNA, in the absence and presence of the core domain D1 or peptides E and F. By monitoring the real-time annealing kinetics of native and mutated fluorescently labelled SL2 and DLS with their respective complementary sequences, the three

peptides were found to promote both annealing reactions and partly switch the loop–loop interaction pathway, which predominates in the absence of peptide, towards a pathway involving the stem termini. Moreover, to site-selectively monitor the effect of the core peptides on the oligonucleotides (ODNs), we introduced 2-aminopurine (2Ap), an environment-sensitive fluorescent nucleoside analogue of adenine (36) at several positions of SL2 and DLS and of their complementary sequences. A comparative analysis of the effects of the various core peptides on the RNA and DNA versions of SL2 further reveals that the chaperone properties are mediated mainly by the interaction between the core basic amino acids and the ODN phosphate backbone.

MATERIALS AND METHODS

Oligonucleotides and core peptides

The unlabelled and labelled ODNs were synthesized by IBA GmbH Nucleic Acids product Supply (Gottingen, Germany). In the case of the doubly labelled ODNs, the 5′ terminus was labelled with carboxytetramethylrhodamine (TMR) or rhodamine 6G (Rh6G) via an amino-linker with a six carbon spacer arm, while the 3′ terminus was labelled with either 4-(4′-dimethylaminophenylazo) benzoic acid (Dabcyl) or 5(and 6)-carboxyfluorescein (Fl) using a special solid support with the dye already attached. ODNs were purified by the manufacturer by reverse-phase HPLC and polyacrylamide gel electrophoresis.

Peptides E and F (Figure 1C) were synthesized by solid phase peptide synthesis on a 433A synthesizer (ABI, Foster City, CA, USA) as described (19). Purification by HPLC was carried out on a C8 column (Uptisphere 300 Å, 5 μm; 250×10, Interchim, France) in 0.05% TFA with a linear gradient of 10–70% of acetonitrile for 30 min. The peptide purity and molecular weight (6754 for peptide E and 9444 for peptide F) were checked by LC/MS. An absorption coefficient of 5700 $M^{-1}\,cm^{-1}$ at 280 nm was used to determine their concentration. The D1 domain (Figure 1C) consisting of amino acids 1–117 of the core protein fused to a C-terminal 6×His-tag was prepared, as previously described (25).

Experiments were performed in 50 mM HEPES–HCl (pH 7.5), 30 mM NaCl and 0.2 mM $MgCl_2$ at 20°C.

Steady-state fluorescence spectroscopy measurements

Emission spectra and kinetic traces were recorded with Fluorolog and FluoroMax spectrofluorimeters (Horiba, Jobin Yvon Instruments) equipped with a temperature-controlled cell compartment. All fluorescence intensities were corrected for buffer emission and lamp fluctuations. Quantum yields of 2Ap-labelled ODNs were calculated using free 2Ap riboside as a reference (0.68) and an excitation wavelength of 315 nm (36).

For the annealing assays, the ODNs were first heated at 80°C for 2 min and then put on ice for 2 min. Real-time kinetic measurements were performed in pseudo first-order conditions by using concentrations of unlabelled cSL2 and cDLS at least 10-fold higher than the concentration of the labelled SL2 and DLS sequences. Excitation and emission wavelengths were 520 and 550 nm, respectively, to monitor the Rh6G fluorescence. The corresponding wavelengths were 480 and 520 nm, respectively, to monitor the Fl fluorescence. All reported concentrations correspond to those after mixing. To avoid high local concentrations during mixing, both reactant mixtures were in the same volume. Peptides were separately added to each reactant at a peptide to ODN ratio of 1:1 and 0.5:1 for SL2 and DLS, respectively, and then the reaction was initiated by mixing the peptide-coated ODNs together. The kinetics was fast enough to monitor the fluorescence intensities continuously without photo-bleaching. The apparent rate constants k_{obs} and the amplitudes were determined from the kinetic traces by including a dead-time correction t_0 to take into account the delay between the mixing of reactants and the start of the measurements. All fitting procedures were carried out with the Origin™ 7.5 software based on non-linear, least-square methods and the Levenberg–Marquardt algorithm.

The temperature dependence of the annealing kinetics was carried out with either 20 nM doubly labelled DLS derivatives and 4 μM non-labelled cDLS derivatives or with 10 nM doubly labelled SL2 derivatives and 200 nM non-labelled cSL2 derivatives at increasing temperatures (15, 20, 25, 30, 35 and 40°C) in the presence of either peptide E, peptide F and domain D1. The same experiments were carried out in the absence of peptide, but only with the SL2/cSL2 system.

RESULTS

Kinetics of SL2/cSL2 and DLS/cDLS annealing

The real-time annealing kinetics of SL2 and DLS with their complementary cSL2 and cDLS sequences (Figure 1D) were investigated by mixing excess of non-labelled cSL2 and cDLS with TMR-5′-SL2-3′-Fl and TMR-5′-DLS-3′-Fl, respectively. Formation of the 27- and 16-bp extended duplex (ED) strongly increases the interchromophore distance, leading to the recovery of Fl emission (28). To determine the fluorescence intensity of the fully stretched ED, we heated the complementary sequences in pseudo-first order conditions at 80°C for 2 min, followed by slow cooling.

A difference of 20- and 12-times was observed for SL2/cSL2 and DLS/cDLS, respectively, between the Fl fluorescence intensities of the initial closed stem–loops and the final extended ED (insets of Figure 2A and B, respectively). The annealing kinetic traces (Figure 2A and B) could be adequately fitted using a biexponential function:

$$I(t) = I_f - (I_f - I_0)(ae^{(-k_{obs1}(t-t_0))} - (1-a)e^{(-k_{obs2}(t-t_0))}) \quad (1)$$

where $I(t)$ is the actual fluorescence intensity at 520 nm, k_{obs1} and k_{obs2} are the apparent pseudo-first order rate constants, a is the relative amplitude of the fast component, and t_0 is the dead time. I_0 and I_f stands for the fluorescence intensities of TMR-5′-DLS-3′-Fl or

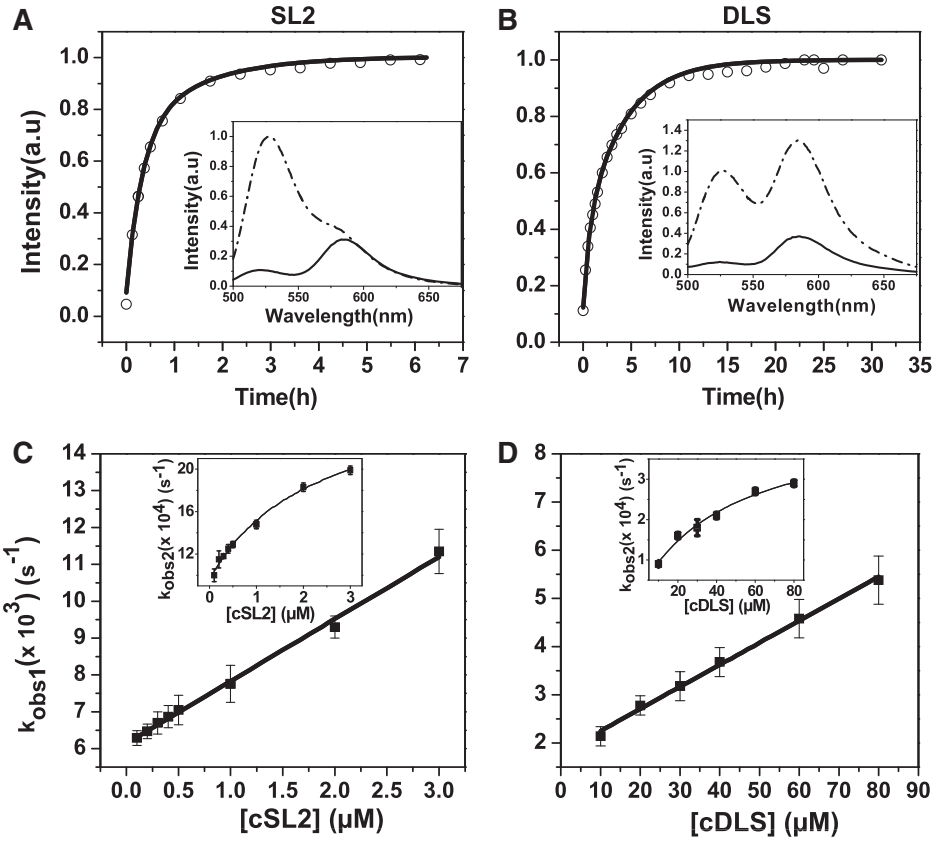

Figure 2. Experimental kinetic curves (**A** and **B**) and parameters (**C** and **D**) of SL2/cSL2 (A and C) and DLS/cDLS (B and D) annealing. (A) Kinetic trace of 10 nM doubly labelled SL2 reacted with 500 nM of unlabelled cSL2 (disks) and its fit with Equation (1) (solid line). Inset: emission spectra of the doubly labelled SL2 before (solid line) and after (dash-dot) completion of the annealing reaction with cSL2. (B) Kinetic trace of 20 nM doubly labelled DLS reacted with 1 μM of unlabelled cDLS (disks), and its fit with Equation (1) (solid line). Inset: emission spectra of the doubly labelled DLS before (solid line) and after (dash-dot) completion of the annealing reaction with cDLS. The fast (k_{obs1}) (C and D) and slow (k_{obs2}) (Insets C and D) components for SL2/cSL2 (C) and DLS/cDLS (D) annealing were determined in pseudo-first-order conditions from real-time kinetics, as described in (A) and (B). The solid lines correspond to the fit of the experimental data (squares) with Equations (2) and (3), using the values given in Tables 1 and 2. Experiments were performed in 50 mM HEPES (pH 7.5), 30 mM NaCl, 0.2 mM $MgCl_2$ at 20°C. Excitation and emission wavelengths were 480 and 520 nm, respectively, to monitor the fluorescein emission.

TMR-5′-SL2-3′-Fl in their free state and in the final ED, respectively.

Interestingly, the fast component, k_{obs1}, linearly varies with cDLS or cSL2 concentrations (Figure 2C and D), while k_{obs2} shows a hyperbolic dependence on the complementary sequence concentration (Figure 2C and D, insets). This behaviour is consistent with a two-step reaction, as described in Scheme 1:

$$\mathrm{SL2 + cSL2} \underset{k_{diss}}{\overset{k_{ass}}{\rightleftharpoons}} \mathrm{IC_S} \underset{k_b}{\overset{k_f}{\rightleftharpoons}} \mathrm{ED_S}$$

or

$$\mathrm{DLS + cDLS} \underset{k_{diss}}{\overset{k_{ass}}{\rightleftharpoons}} \mathrm{IC_D} \underset{k_b}{\overset{k_f}{\rightleftharpoons}} \mathrm{ED_D}$$

Scheme 1. Proposed reaction scheme for SL2/cSL2 and DLS/cDLS annealing reactions

where a fast pre-equilibrium intermediate, IC, precedes the formation of the final stable ED through a monomolecular reaction (33). Formation of IC is governed by the second order association rate constant, k_{ass}, and the first order dissociation rate constant, k_{diss}, while the interconversion of IC into ED is governed by the forward and backward interconversion rate constants, k_f and k_b. The hyperbolic dependence of k_{obs2} on the concentration of non-labelled complementary ODNs may be associated to IC accumulation as a consequence of its slow inter-conversion into ED which is likely the rate-limiting step of the annealing reaction. If the pre-equilibrium is rapidly reached (k_{ass}[cDLS-or-cSL2]+$k_{diss} >> k_f$), Scheme 1 predicts a linear variation of k_{obs1}, which can thus be described by:

$$k_{obs1} = k_{ass}[\mathrm{cDLS - or - cSL2}] + k_{diss} \quad (2)$$

On the other hand, the hyperbolic variation of k_{obs2} on the complementary ODN concentration can be described by:

$$k_{obs2} = \frac{k_f K_M[\mathrm{cDLS - or - cSL2}]}{1 + K_M[\mathrm{cDLS - or - cSL2}]} + k_b \quad (3)$$

where K_M is the equilibrium association constant governing the IC formation ($K_M = k_{ass}/k_{diss}$).

Table 1. Kinetic parameters of SL2/cSL2 annealing and their mutants in the absence and presence of core peptides

ODN	Fluorophores	Complementary ODN	Peptide	Ratio of peptide/ODN	k_{ass} ($M^{-1}s^{-1}$) $\times 10^{-3}$	k_{diss}.(s^{-1}) $\times 10^{4}$	K_M (M^{-1}) $\times 10^{-5}$	k_f (s^{-1}) $\times 10^{3}$
SL2	3′Fl–5′TMR	cSL2	–	–	1.7 (±0.04)	62 (±6)	4.4 (±1)	1.8 (±0.2)
SL2	3′Fl–5′TMR	cSL2-Stem	–	–	1.4 (±0.08)	43 (±5)	4.3 (±1)	2.2 (±0.2)
SL2	3′Fl–5′TMR	cSL2-Zip	–	–	1 (±0.06)	18.3 (±2)	2.6 (±1)	1.1 (±0.2)
SL2	3′Fl–5′TMR	cSL2-Loop	–	–	0.09 (±0.002)	15.1 (±0.4)	0.8 (±0.6)	1.5 (±0.2)
SL2-Loop	3′Fl–5′TMR	cSL2	–	–	0.1 (±0.006)	10.1 (±0.8)	0.9 (±0.2)	0.82 (±0.06)
SL2	3′Fl–5′TMR	cSL2	E	1	56 (±3)	90 (±20)	39 (±10)	19 (±0.1)
SL2	3′Fl–5′TMR	cSL2-Stem	E	1	31 (±2)	86 (±6)	22 (±3)	17 (±0.4)
SL2	3′Fl–5′TMR	cSL2-Zip	E	1	23 (±0.8)	67 (±6)	33 (±10)	6 (±0.4)
SL2	3′Fl–5′TMR	cSL2-Loop	E	1	13 (±0.8)	60 (±6)	28 (±10)	1.6 (±0.1)
SL2-Loop	3′Fl–5′TMR	cSL2	E	1	27 (±3)	280 (±25)	8 (±1)	3 (±1)
SL2-DNA	3′Rh6G–5′Dabcyl	cSL2-DNA	–	–	1.3 (±0.1)	41 (±8)	3.5 (±1)	2.6 (±0.3)
SL2-DNA	3′Rh6G–5′Dabcyl	cSL2-DNA	E	1	98 (±7)	173 (±5)	43 (±7)	10 (±0.4)
SL2	3′Fl–5′TMR	cSL2	D1	1	31 (±2)	280 (±6)	13 (±5)	16 (±3)
SL2	3′Fl–5′TMR	cSL2	F	1	310 (±10)	86 (±20)	380 (±20)	21 (±0.5)

Kinetic rate constants were calculated from the dependence of the k_{obs} values on the concentration of the unlabelled ODN, as indicated in Figure 2. The k_{ass} and k_{diss} values were calculated with Equation (2), while the K_M and k_f values were calculated using Equation (3). The K_M values were found to differ by a factor of <2 from the k_{ass}/k_{diss} values, which further supports the proposed reaction Scheme 1.

Table 2. Kinetic parameters of DLS/cDLS annealing and their mutants in the absence and presence of core peptides

ODN	Fluorophores	Complementary ODN	Peptide	Ratio of peptide/ODN	k_{ass} ($M^{-1}s^{-1}$) $\times 10^{-3}$	k_{diss} (s^{-1}) $\times 10^{4}$	K_M (M^{-1}) $\times 10^{-5}$	k_f (s^{-1}) $\times 10^{3}$
DLS	3′Fl–5′TMR	cDLS	–	–	0.46 (±0.01)	180 (±8)	0.21 (±0.07)	0.44 (±0.05)
DLS	3′Fl–5′TMR	cDLS	E	0.5	2.7 (±0.2)	89 (±4)	2.2 (±0.6)	5.4 (±0.7)
DLS	3′Fl–5′TMR	cDLS-Stem	E	0.5	2 (±0.1)	92 (±4)	2.1 (±0.6)	6.3 (±0.3)
DLS	3′Fl–5′TMR	cDLS-Loop	E	0.5	56 (±4)	95 (±8)	45 (±20)	50 (±20)
DLS-Loop	3′Fl–5′TMR	cDLS	E	0.5	1.4 (±0.1)	168 (±30)	0.85 (±0.1)	3 (±1)

Kinetic rate constants were calculated from the dependence of the k_{obs} values on the concentration of the unlabelled ODN, as indicated in Figure 2. The k_{ass} and k_{diss} values were calculated with Equation (2), while the K_M and k_f values were calculated using Equation (3). The K_M values were found to differ by a factor of <2 from the k_{ass}/k_{diss} values, which further supports the proposed reaction Scheme 1.

The k_{ass} values for both SL2/cSL2 ($1.7 \times 10^3 M^{-1} s^{-1}$) and DLS/cDLS ($4.6 \times 10^2 M^{-1} s^{-1}$) (Tables 1 and 2) annealing reactions were several orders of magnitude smaller than the 10^5–$10^7 M^{-1} s^{-1}$ rate constants reported for the annealing of unstructured sequences (37). This suggests that for both reactions, there is a low probability of the ODNs to be melted at room temperature and to nucleate the duplex upon collision (38). Moreover, the values of k_b, given by intercepts, were found to be close to zero indicating that the dissociation of ED is negligible. This is in line with the large differences in the stability of the ED and the initial stem–loops.

To further check the validity of the postulated two-step annealing mechanism, we used the Dynafit numerical resolution software (39), which allows fitting simultaneously the experimental progress curves, obtained at different complementary ODN concentrations. The best estimates of the elementary rate constants k_{ass}, k_{diss} and k_f (Supplementary Table S1) were in excellent agreement with those found by the empirical approach (Tables 1 and 2), further strengthening the proposed reaction scheme.

To get further insight in the annealing mechanism, we evaluated the temperature dependence of the k_{obs} values of SL2/cSL2 annealing kinetics by using the Arrhenius equation:

$$k_i = A_i \exp\left(\frac{E_{a,i}}{RT}\right) \quad (4)$$

where the rate constant k_i is given by k_{obsi}/[cSL2], A_i is the pre-exponential Arrhenius factor, $E_{a,i}$ is the activation energy, R is the universal gas constant and T is the temperature (in Kelvin).

For the SL2/cSL2 annealing, both reaction rates were found to increase with temperature (Figure 3A and B), providing positive values for the transition state enthalpies of 4.8(± 0.7) kcal mol^{-1} and 14.5(± 2) kcal mol^{-1}, for the fast and slow components, respectively. These enthalpy values suggest that the SL2/cSL2 annealing reaction involves premelting of 1 and 3 bp, for the fast and slow kinetic components, respectively (40,41).

Dependence of the annealing kinetics on the oligonucleotide sequence

To further characterize the molecular mechanism of the SL2/cSL2 annealing, we analysed the annealing kinetics with different SL2 and cSL2 mutants (Figure 1D).

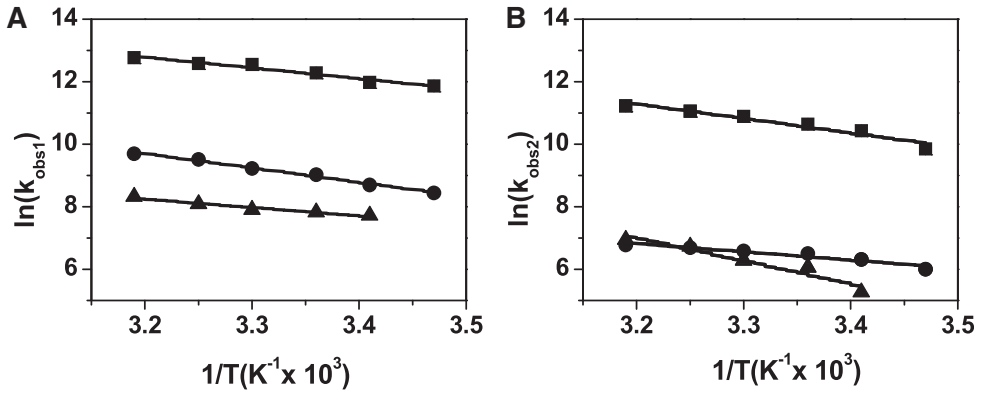

Figure 3. Temperature dependence of SL2/cSL2 and DLS/cDLS annealing kinetics. The natural logarithms of the rate constant values for the fast (**A**) and slow (**B**) components of the SL2/cSL2 and DLS/cDLS annealing reactions were plotted as a function of the inverse of the temperature. The SL2/cSL2 annealing reactions were monitored either in the absence of peptide E, by mixing 10 nM doubly labelled SL2 with 6 μM unlabelled cSL2 (triangles) or in the presence of peptide E at a peptide to oligonucleotide ratio 1:1 by mixing 10 nM TMR-3′-SL2-5′-Fl with 200 nM cSL2 (squares). The DLS/cDLS annealing reaction was performed only in the presence of peptide E at a peptide to oligonucleotide ratio of 0.5:1, with 20 nM doubly labelled DLS and 4 μM non-labelled cDLS (disks). The solid lines are the best fits to Equation (4). The values of the transition state enthalpies given in Table 3 were calculated from the activation energies E_a given by the fits, using $\Delta H^* = Ea - RT$ with $T = 293.15$ K.

Table 3. Arrhenius parameters of the annealing of SL2/cSL2 and DLS/cDLS in the absence and the presence of peptide E

ODN	Fluorophores	Complementary ODN	Ratio of peptide E/ODN	ΔH (Fast) (kcal mol^{-1})	ΔH (Slow) (kcal mol^{-1})
SL2	3′Fl–5′TMR	cSL2	0	4.8 (±0.7)	14.5 (±2)
SL2	3′Fl–5′TMR	cSL2-Stem	0	4.2 (±0.9)	15.5 (±2)
SL2	3′Fl–5′TMR	cSL2-Zip	0	8.9 (±0.5)	11 (±1)
SL2	3′Fl–5′TMR	cSL2-Loop	0	25.5 (±3)	7.9 (±0.8)
SL2-Loop	3′Fl–5′TMR	cSL2	0	11 (±1)	10.1 (±0.5)
SL2	3′Fl–5′TMR	cSL2	1	8.3 (±0.6)	9 (±1)
SL2	3′Fl–5′TMR	cSL2-Stem	1	7.2 (±0.9)	15 (±1)
SL2	3′Fl–5′TMR	cSL2-Zip	1	7.9 (±0.5)	13 (±1)
SL2	3′Fl–5′TMR	cSL2-Loop	1	11.6 (±0.6)	12 (±1)
SL2-Loop	3′Fl–5′TMR	cSL2	1	12.2 (±0.6)	12.5 (±2)
DLS	3′Fl–5′TMR	cDLS	0.5	8.6 (±0.2)	4.7 (±0.7)
DLS	3′Fl–5′TMR	cDLS-Stem	0.5	9 (±0.2)	9.2 (±0.4)
DLS	3′Fl–5′TMR	cDLS-Loop	0.5	5.7 (±0.6)	4.8 (±0.6)
DLS-Loop	3′Fl–5′TMR	Cdls	0.5	16 (±2)	19 (±1.5)

The values of the transition state enthalpy ΔH^* for the fast and slow pathways were calculated from the fits of the temperature dependence of the k_{obs} values to Equation (4), as described in Figure 3.

To investigate the role of the stem in the annealing reaction, we used the cSL2-Stem mutant in which the last and penultimate base pairs at the bottom of the stem were inverted, in order to prevent base pairing with SL2 through the stem termini. These mutations only marginally changed the values of the kinetic parameters (Table 1 and Supplementary Figure S1A) and the transition state enthalpy (Table 3), suggesting that the stem termini play a minor role in the nucleation of the SL2/cSL2 annealing reaction. Next, to determine whether the annealing was nucleated through loop–loop interactions, we used the SL2-Loop and cSL2-Loop mutants, where the $A_{16,\ 17\ and\ 18}$ and C_{13}, A_{14}, C_{15} residues, respectively, were changed to U residues (Figure 1D) in order to decrease the complementarities between the central loops. For both the SL2-Loop/cSL2 and SL2/cSL2-Loop annealing reactions, an ~20-fold decrease in the k_{ass} value was observed. This decrease in the k_{ass} value was partly compensated by a 4- to 6-fold decrease in the k_{diss} value, leading to a 5-fold decrease in the K_M value. These changes in the kinetic parameters associated to the fast component were coupled with a strong increase in the value of the transition state enthalpy (Table 3), which was more pronounced for the SL2/cSL2-loop reaction. These important changes in the annealing parameters with the loop mutants strongly suggest that the SL2/cSL2 annealing reaction is mainly nucleated through the loops and that the SL2-Loop/cSL2 and SL2/cSL2-Loop reactions follow a different pathway. Interestingly, the high values of the transition state enthalpy (25.5 and 11 kcal mol^{-1}) for the fast component of the SL2/cSL2-Loop and SL2-Loop/cSL2 annealing reactions were consistent with the melting of 3–6 bp, suggesting that in these reactions, annealing could be nucleated through the stem. In addition, a significant decrease in the fluorescence plateau was observed for both the SL2-Loop/cSL2 and SL2/cSL2-Loop annealing reactions as compared to the SL2/cSL2 annealing (Supplementary Figure S1A). This fluorescence plateau was independent on the concentration of the complementary sequence, and thus could not

be related to an incomplete reaction between partners. A more likely explanation is that the partial complementarity between the loops induces some flexibility in the middle of the ED, allowing its kinking and thus a closer distance between the probes at the opposite ends of the duplex.

Finally, to investigate the contribution of the internal loop in the annealing reaction, we used the cSL2-Zip mutant, in which the A_{20} and G_{21} residues were substituted by U residues (Figure 1D) in order to prevent base pairing with the complementary residues of the SL2 internal loop. An ~2-fold decrease in the kinetic parameters as well as a 2-fold increase in the transition state enthalpy associated to the fast component were observed with this mutant with respect to the native cSL2 sequence (Table 1). These data suggest that the internal loop contributes to the nucleation and stability of the IC, as well as its further conversion into ED. Next, we checked if changing the ribose backbone to deoxyribose had any impact on the kinetic parameters. To this end, we repeated the annealing experiments with the DNA version of SL2 and cSL2 sequences. Results (Table 1) indicated that the nature of the nucleotide backbone marginally influences the kinetic parameters and thus, the annealing mechanism.

Taken together, our data suggest that the SL2/cSL2 annealing reaction is mainly nucleated through interaction of the central and internal loops. Thus, the IC probably involves an extended kissing loop between residues 7–21 of SL2 and cSL2. Formation of the IC requires the melting of the upper double stranded segment, which may well correspond to the transition state enthalpy ($4.8\,kcal\,mol^{-1}$) associated to the fast kinetic component. A second pathway through the stem termini was revealed when the loops were mutated. However, this pathway is likely minor in the SL2/cSL2 reaction, since mutation of the stem termini only induces marginal changes in the reaction kinetics.

The very slow rates of the DLS/cDLS annealing reaction even at very high concentrations of complementary sequences prevented us to determine the full set of kinetic parameters. Nevertheless, experiments at a single concentration of DLS with the cDLS-Stem mutant (where the last and penultimate base pairs at the bottom of the stem were inverted, Figure 1) indicated that almost no changes occurred in the reaction rates as compared to the reaction with the native sequences (Supplementary Figure S1B). In sharp contrast, a strong decrease in the reaction rate as well as a decrease in the fluorescence plateau were observed when cDLS was reacted with the doubly labelled DLS-Loop mutant, in which the A_9 and G_{10} residues were substituted by U nucleotides (Figure 1), indicating that the DLS/cDLS annealing reaction, like SL2/cSL2, is also mainly nucleated through loop–loop interactions.

Kinetics of SL2/cSL2 and DLS/cDLS annealing in the presence of core peptide E

To characterize the mechanism by which the core protein can activate the annealing of SL2/cSL2 and DLS/cDLS, we first used peptide E, which mimics the core chaperone properties and can be synthesized in large quantities (19,26,27). Addition of peptide E to the labelled SL2 or DLS sequences did not lead to any change in their fluorescence spectrum (Figure 4A and B, insets), indicating that peptide E was unable to destabilize their secondary structure, as already reported with the cTAR model sequence (27). Annealing reactions were then performed by adding peptide E at a peptide to nucleotide ratio of 1:1 and 0.5:1 to SL2/cSL2 and DLS/cDLS systems, respectively, in order to ensure aggregation-free conditions. A rapid increase in the fluorescence was observed when the doubly labelled SL2 and DLS were mixed with their complementary cSL2 and cDLS sequences in the presence of peptide E. The final fluorescence reached the same plateau value as in the absence of core peptide (Figure 2A and B), suggesting that the reaction went to completion giving the same ED.

Interestingly, peptide E caused a dramatic increase in the reaction kinetics, as the reactions for both systems were completed much faster as compared to their respective reactions in its absence (compare Figure 2A and B with Figure 4A and B). As in the absence of peptide, the kinetic traces could be adequately fitted with Equation (1). Furthermore, like in the absence of core, the fast component, k_{obs1}, varied linearly with [cSL2 or cDLS], while k_{obs2} showed a hyperbolic dependence (Figure 4C and D), suggesting a similar two-step reaction mechanism (Scheme 1). For both systems, peptide E was found to increase the values of k_{ass}, k_f and K_M by about one order of magnitude, while the k_{diss} value remained almost unchanged (Tables 1 and 2). The values of k_b for both annealing reactions were found to be very low ($<10^{-4}\,s^{-1}$), indicating that peptide E is unable to dissociate the ED. Thus, on the basis of the kinetic data, the same reaction mechanism as described in Scheme 1 can also be proposed for peptide E-promoted SL2/cSL2 and DLS/cDLS annealing. The validity of this reaction mechanism was further checked with the Dynafit numerical resolution software (Supplementary Table S1).

Finally, we studied the reaction mechanism by analysing the temperature dependence of the k_{obs} values. Analysis of both reaction rates at increasing temperatures (Figure 3) provided positive enthalpy values (Table 3) for peptide E-promoted SL2/cSL2 and DLS/cDLS annealing. These enthalpy values indicated that peptide E-promoted SL2/cSL2 annealing involves premelting of 2 to 3 pb, for both kinetic components (40,41), while peptide E-promoted DLS/cDLS annealing involves premelting of 2–3 and 1–2 bp, for the fast and slow kinetic components, respectively.

Dependence of the core peptide E-promoted annealing kinetics on the oligonucleotide sequence

To get further insight into the molecular mechanism of the peptide E-promoted-SL2/cSL2 annealing, SL2 and cSL2 mutants were used. Substitution of cSL2 by the cSL2-Stem mutant induced a 2-fold decrease in the k_{ass} and K_M values, suggesting that the bottom of the stem contributes to the formation and stability of the IC (Table 1 and Supplementary Figure S2A). Moreover, a

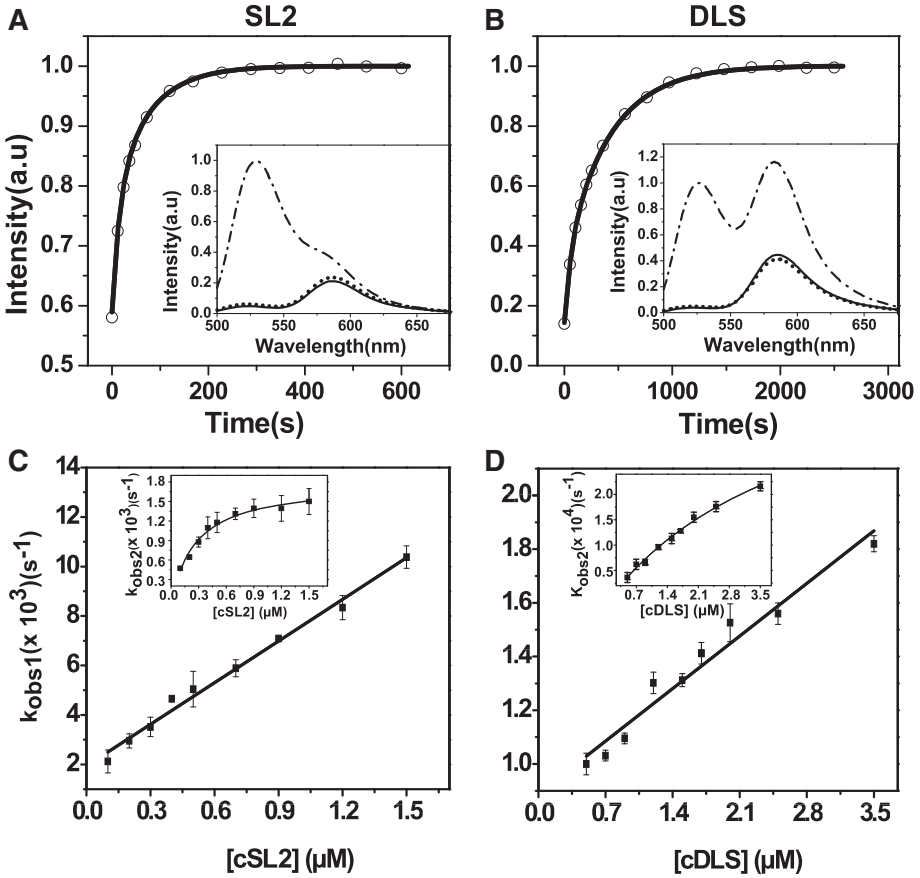

Figure 4. Experimental kinetic curves (**A** and **B**) and parameters (**C** and **D**) of SL2/cSL2 (A and C) and DLS/cDLS (B and D) annealing in the presence of peptide E. (A) Kinetic trace of 10 nM doubly labelled SL2 with 500 nM of unlabelled cSL2 (disks) and its fit with Equation (1) (solid line). Inset A: emission spectra of the doubly labelled SL2 before (solid line) and after (dash-dot) completion of the annealing reaction with cSL2. The emission spectrum of the doubly labelled SL2 in the presence of peptide E (dot) shows marginal destabilization of SL2 by peptide E. (B) Kinetic trace of 20 nM doubly labelled DLS with 3 μM of unlabelled cDLS (disks) and its fit with Equation (1) (solid line). Inset B: emission spectra of the doubly labelled DLS before (solid line) and after (dash-dot) completion of the annealing reaction with cDLS. The emission spectrum of the doubly labelled DLS in the presence of peptide E (dot) shows marginal destabilization of DLS by peptide E. The fast (k_{obs1}) (C and D) and slow (k_{obs2}) (Insets C and D) components were determined as described in Figure 2 and fitted with Equations (2) and (3) (solid lines), using the values given in Tables 1 and 2. Experiments were performed in 50 mM HEPES (pH 7.5), 30 mM NaCl, 0.2 mM $MgCl_2$ at 20°C with peptide E added at a peptide to oligonucleotide ratio of 1:1 and 0.5:1 for SL2/cSL2 and DLS/cDLS annealing, respectively. Excitation and emission wavelengths were 480 and 520 nm, respectively, to monitor the fluorescein emission.

moderate increase from 9 to 15 kcal mol^{-1} was observed for the transition enthalpy energy of the slow component, suggesting that this component was related to the melting of the stem. A 2-fold decrease in the k_{ass} value, associated to a limited decrease in the K_M value and a 3-fold decrease in the k_f value were observed with the cSL2-Zip mutant, suggesting that the internal loop is probably involved in the IC formation and its conversion into ED.

Furthermore, the cSL2-Loop and SL2-Loop mutations induced a 2- to 5-fold decrease in the k_{ass} and K_M values, a 3- to 4-kcal mol^{-1} increase in the values of the transition enthalpy for both the slow and fast components and more prominently a 6- to 10-fold decrease in the k_f value (Table 1), suggesting that the loops play an important role in the formation of the IC and its further conversion into the ED. Interestingly, comparison of the kinetic parameters in the absence and presence of peptide revealed that peptide E increased the k_{ass} and K_M values of both the SL2/cSL2-Loop and SL2-Loop/cSL2 reactions by two and one order of magnitude, respectively. Thus, for both annealing reactions, peptide E prominently promotes the reaction pathway through the stem termini, which already exists in the absence of peptide. This promotion is mainly achieved by activating the IC formation. A strong promotion by peptide E of the pathway through the stem termini likely occurs also in the SL2/cSL2 annealing reaction, so that this pathway becomes more or less of equal importance to the pathway through the loops, as suggested by the reduction by a factor of two of the k_{ass} and K_M values with the cSL2-Stem mutant. Finally, the annealing experiments with the DNA version of SL2 and cSL2 indicated that the nature of the nucleotide backbone does not strongly affect peptide E-promoted annealing (Table 1).

We then investigated the molecular determinants for peptide E-promoted DLS/cDLS annealing. Substitution

of cDLS by the cDLS-Stem mutant induced a moderate decrease in the k_{ass} value, but did not significantly change the other kinetic parameters (Table 2 and Supplementary Figure S2B), suggesting that the stem termini do not play a key role in the annealing reaction. Moreover, similar to peptide E-promoted SL2/cSL2-Stem annealing, an increased value of the transition state enthalpy was observed for the slow kinetic component (Table 3) of the annealing with the cDLS-Stem mutant, suggesting that the conversion of IC into ED involves melting of the stem.

Surprisingly, substitution of cDLS by the cDLS-Loop mutant in which A_9 and G_{10} were substituted by U nucleotides (Figure 1) was found to increase the k_{ass}, K_M and k_f values by about one order of magnitude as compared to those observed with DLS/cDLS (Table 2). These large changes in the annealing kinetics suggest that the loop plays a key role in DLS/cDLS annealing and that structural constraints in the native cDLS loop likely restrict its annealing with the DLS loop, as well as the conversion of the IC into the ED. These structural constraints possibly arise from base-pairing between the ^{6}C–G^{7} and the ^{10}C–G^{11} nucleotides in the 8-nt loop of the native cDLS sequence. In contrast, substitution of G_{10} by U in the cDLS-loop mutant can prevent such base pairing and thus favour an efficient annealing of the resulting flexible mutated loop with DLS. This hypothesis is supported by the decreased stability of the mutated loop sequence as compared to the native loop in cDLS, as suggested by the decreased value of the transition state enthalpy (Table 3) for the fast kinetic component, which indicates a lower energy barrier for nucleating the IC. Moreover, the transition enthalpy for the slow component was identical to that observed with the native cDLS, suggesting that melting of the stem constitutes the rate-limiting step in both sequences.

To confirm the key role of the loops in the annealing reactions, we mutated the loop of DLS, by substituting the A_9 and G_{10} residues with U residues. In contrast to the cDLS mutant, we observed a 2- to 3-fold decrease in k_{ass}, K_M and k_f values (Table 2) together with a strong increase in the values of the transition state enthalpy (Table 3) for both the fast and slow kinetic components, as compared to the peptide E-promoted-DLS/cDLS annealing reaction. These data confirmed the key role of the loops in the peptide E-promoted annealing reaction of DLS with cDLS. The high values (16 and 19 kcal mol^{-1}) of the transition state enthalpy for both the fast and slow components suggest that the annealing of the DLS-Loop mutant with cDLS may be initiated through the stem. In this respect, the fast component may be associated with the melting of the 3 bp at the stem bottom, while the slow component may be associated with the energy needed for the melting of the remaining base pairs of the stem and the conformational changes associated with the conversion of the IC into the ED.

Taken together, our data indicate that peptide E can promote DLS/cDLS and SL2/cSL2 annealing reactions through both a loop–loop interaction pathway and a pathway involving the stem termini.

SL2/cSL2 annealing promoted by the core peptide F and domain D1

Next, we investigated the effect of the other two core peptides (peptide F and D1 domain) on the annealing of SL2 with cSL2, to determine whether they promote the annealing reaction through the same mechanism as peptide E (Figure 1C). The annealing kinetics in their presence was also biphasic with a linear and hyperbolic dependence of k_{obs1} and k_{obs2}, respectively, on the concentration of cSL2 (Table 1), suggesting that the three core peptides promote SL2/cSL2 annealing by the same mechanism. We observed marked differences in the k_{ass} and K_M values with peptide F and D1 domain as compared to peptide E. While a 2- to 3-fold decrease of the values for both parameters was observed with the D1 domain (Table 1), an increase of about one order of magnitude was observed for peptide F (Table 1). In contrast, the k_f values for the three peptides were similar. Thus, the three peptides promote and stabilize the IC at different levels, but once this complex is formed, it is converted with similar kinetics and thus, through the same mechanism by the three peptides into the ED. The increased k_{ass} and K_M values observed with peptide F as compared to peptide E could be attributed to its additional basic domain that further screens the negative charges of the ODNs and thus, favour their annealing. In contrast, the opposite effect observed with the D1 domain is probably related to its additional neutral Trp-rich domain, which reduces the density of positive charges on the peptide, and thus the ability to screen efficiently the ODN charges. Alternatively, the Trp residues of the Trp-rich domain may stack with the nucleotide bases, and induce structural constraints that limit the electrostatic interactions between the positively charged basic domain of D1 and the negatively charged phosphate groups of the ODNs.

Effect of the core peptide on the dynamics of the 2Ap-labelled HCV oligonucleotides

Site-selective interactions of peptide E with SL2 and DLS were monitored by using ODNs labelled with 2Ap, a fluorescent analogue of adenine, highly sensitive to the environment. To this end, we substituted A residues by 2Ap in DLS and cDLS at position 9 (DLS_{9Ap} and $cDLS_{9Ap}$) as well as in SL2 at position 3 ($SL2_{3Ap}$), 9 ($SL2_{9Ap}$) and 16 ($SL2_{16Ap}$) and cSL2 at position 3 ($cSL2_{3Ap}$), 14 ($cSL2_{14Ap}$) and 20 ($cSL2_{20Ap}$) (Figure 5A). In the absence of peptide E, the 2Ap-labelled ODNs exhibit a rather low quantum yield, as a consequence of the dynamic quenching of 2Ap fluorescence by the neighbouring bases (42,43), and notably the flanking G residues which are the strongest quenchers among the nucleobases (44).

Binding of peptide E to the various 2Ap-labelled ODNs caused marginal changes in the quantum yield (Figure 5B) and emission maximum (data not shown), suggesting that peptide E does not restrict the dynamic interactions of the 2Ap residues with their neighbouring bases in the central loop of SL2, DLS and cDLS and the internal loop of SL2 and cSL2. The absence of any effect of the peptide on the central and internal loops of these ODNs can hardly be connected with an absence of binding of peptide E to these

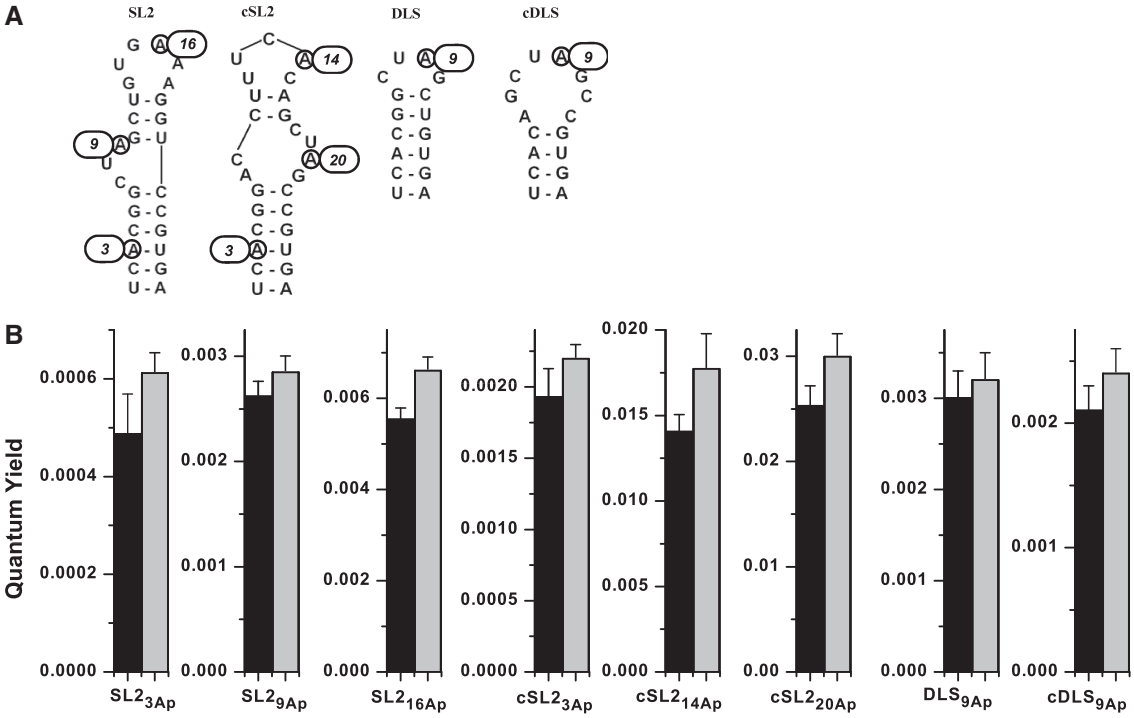

Figure 5. Site-selective monitoring of the interaction of peptide E with 2-Ap-labelled SL2, cSL2, DLS and cDLS sequences. (**A**) Labelled positions in HCV oligonucleotides. The SL2 and cSL2 sequences were labelled by 2-Ap in the stem (at position 3), the internal loop (at position 9 and 20 for SL2 and cSL2, respectively) and the central loop (at position 16 and 14 for SL2 and cSL2, respectively). The DLS and cDLS sequences were labelled by 2-Ap in the loop (at position 9). (**B**) Quantum yields of $SL2_{3Ap}$, $SL2_{9Ap}$, $SL2_{16Ap}$, $cSL2_{3Ap}$, $cSL2_{14Ap}$, $cSL2_{20Ap}$, DLS_{9Ap} and $cDLS_{9Ap}$ in the absence (black bar) and presence (grey bar) of peptide E. Quantum yields were calculated assuming a quantum yield of 0.68 for free 2Ap (42). Excitation wavelength was 315 nm. Experiments were performed in 50 mM HEPES (pH 7.5), 30 mM NaCl, 0.2 mM $MgCl_2$ at 20°C.

regions, since the annealing reaction was shown to be promoted by peptide E through interactions of these regions. A more likely explanation is that by analogy to the unfolded and fingerless mutant of the NCp7 protein of HIV-1 (42,45), peptide E may only bind to the negatively charged phosphate groups of the ODNs, but not to their bases.

DISCUSSION

RNA chaperone proteins are vital partners of RNA in viruses where they are thought to chaperone the correct folding and structural rearrangements of RNA molecules by resolving misfolded kinetically trapped RNA species in an ATP-independent manner (34,35). At various stages of their cellular journey, that includes transcription, transport, translation and storage, RNA molecules are associated with a particular set of chaperone molecules that protect them and facilitate their folding process (34,46). Moreover, to accomplish its functions, the viral genomic RNA relies, at least in part, on short specific *cis*-acting RNA elements (CREs) (4,46,47). In the case of HCV, the genomic RNA contains a short highly conserved palindromic CRE at its very 3′ end, named DLS, mediating *in vitro* dimerization of the genomic RNA 3′-UTR upon core binding (19,26). The aim of the present work was to characterize the mechanism by which the HCV core chaperones the annealing of DLS and SL2 sequences with their complementary counterparts. To this end, we monitored in real-time conditions, the annealing of these RNA sequences in the absence and presence of different core peptides (D1 domain, peptide E and F).

Without core peptide, the annealing of SL2 with cSL2 and DLS with cDLS was rather slow, taking several hours to reach completion (Tables 1 and 2; Figure 1). This slow annealing kinetics can be related with the requirement of the complementary sequences to be in a reactive conformation and proper orientation in order to nucleate the intermediate complex. Using SL2 mutants, we found that the annealing reaction was mainly initiated through central and internal loops, providing an extended kissing loop intermediate that further converts into the final ED. Formation of the SL2/cSL2 intermediate involves an enthalpy energy of $\sim$4.8 kcal mol^{-1} that corresponds to the melting of the C_{11}–G_{20} base pair and the non-canonical flanking G_{10}–U_{21} and U_{12}–U_{19} base pairs. The rather low energy associated to the melting of these 3 bp suggest that the simultaneous annealing of the central and internal loops may destabilize these base pairs and favour their subsequent thermal melting. This conclusion is substantiated by the much larger transition enthalpy energy (8.9 kcal mol^{-1}) observed when the internal loop was mutated. The resulting IC could be stabilized by up to 15 intermolecular base pairs (Figure 6A). However, the actual number of base pairs in the IC is likely less, as a consequence of steric constraints imposed by the stem.

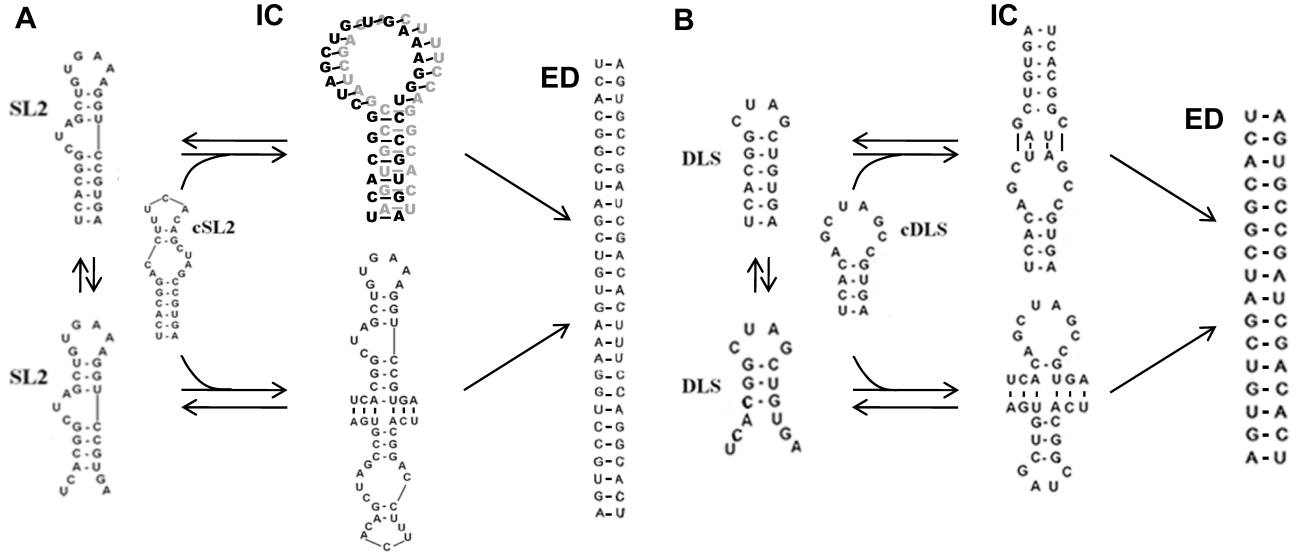

Figure 6. Proposed mechanism for the SL2/cSL2 (**A**) and DLS/cDLS (**B**) annealing reactions. With both SL2 and DLS molecules, thermal fraying likely results in a fast equilibrium between closed species and partially melted species. Annealing reactions are thought to involve two parallel pathways. The upper pathway is thought to be nucleated through loop–loop interaction, while the lower one is thought to be nucleated through the stem termini. In the absence of core protein, the upper pathway is the major one for SL2/cSL2 and DLS/cDLS annealing. The core protein activates the two pathways, but the activation is stronger for the lower pathway, so that the two pathways become of comparable importance. For SL2/cSL2 and DLS/cDLS annealing reactions, the values of the kinetic rate constants given in Tables 1 and 2 are a function of the values of the real kinetic rate constants governing the parallel pathways.

The IC is then converted into the ED in a rate-limiting step associated with a transition enthalpy energy of $\sim$14.5 kcal mol^{-1}, that likely corresponds to the melting of the three stable C–G base pairs in the upper part of the remaining stem. This melting is probably the bottleneck for the interconversion into ED. Interestingly, the somewhat lower transition enthalpy energy (11 kcal mol^{-1}) associated to the slow component for the SL2/cSL2-Zip reaction may be explained by the internal loop that forms at the bottom of the kissing loop, as a result of the mutated nucleotides at positions 20 and 21 in cSL2-Zip. This internal loop in the kissing IC likely destabilizes the stem, explaining the lower energy needed to melt the upper base pairs.

A parallel pathway nucleated through the stem termini was evidenced with the SL2-Loop and cSL2-Loop mutants. The rather high enthalpy energies associated with the fast component of the annealing reactions with these mutants, indicate that a rather large number of base pairs should be pre-melted in the stem of these mutants to nucleate the IC formation. This melting is likely a consequence of the thermal fraying that occurs spontaneously at room temperature. Since fraying occurs in the microsecond to millisecond range (48,49), the equilibrium between the closed and frayed species is thought to be fast, in comparison with the other kinetic steps in Figure 6. With the native SL2 and cSL2 sequences, the pathway through the stem ends appears to play a limited role, since inversion of the two terminal base pairs in cSL2 led only to marginal changes in the annealing reaction.

Similar conclusions were inferred for the DLS/cDLS annealing reaction, with the formation of a kissing loop IC that further converts into the final ED.

The core peptides were found to activate the annealing of SL2/cSL2 and DLS/cDLS, as shown by the one order of magnitude increase in the values of k_{ass}, K_M and k_f in (Tables 1 and 2). This activation resembles that obtained for the annealing of HIV-1 TAR with cTAR by NC protein. Using SL2 and DLS mutants, we found that for both SL2/cSL2 and DLS/cDLS annealing reactions, peptide E promoted the two pathways that already existed in the absence of peptide (Figure 6B). Nevertheless, the promotion was more pronounced for the pathway through the stem termini, since in the presence of core peptides, this pathway became equivalent to that through the loops. The promotion of the pathway through the stem termini may be a result of the thermally driven fraying of SL2 termini and binding of the core protein to the frayed ends. Thus, like for the TAR/cTAR system, where the core protein shifted the annealing mechanism from a kissing loop pathway to a zipper pathway through the stem termini (27), we observe a similar shift in the mechanistic pathways when the core was added to the SL2/cSL2 or DLS/cDLS systems. In fact, the core protein, like other viral proteins such as NCp7 or Tat, may facilitate the annealing of both systems by promoting the attraction between the core-coated complementary ODNs, which favours the diffusional search for the complementary sequences. A second key issue in the core-promoted annealing is related to the enhancement of the interconversion rate. The protein likely favours the conformational rearrangement and the melting of base pairs, which are required for converting the IC into the ED. This role of the protein on the melting of IC base pairs is assessed by the significant decrease in the enthalpy energy associated to the

interconversion step in its presence as compared to its absence. The mechanism of core in the activation of both annealing reactions is in line with the 'entropy exchange model' in which a highly flexible protein, like core, undergoes disorder-to-order transition upon binding to RNA that in turn leads to the melting of the RNA structure through an entropy exchange process (50).

Using 2Ap-labelled ODNs to monitor, at the nucleotide level, the effect of the core protein, we found that the core did not modify the dynamics of the bases in the central and internal loop of SL2, cSL2, DLS or cDLS. This observation is in contrast with the effect of the nucleocapsid protein NCp7, which freezes the local mobility of the bases through interaction with its hydrophobic aminoacids (42,45,51). This suggests that by analogy to the fingerless unfolded mutant of NCp7 (42), peptide E probably interacts with the ODNs mainly through electrostatic interactions between its basic amino acids and the negatively charged phosphate groups, leaving the bases unaffected (27). Moreover, using the DNA version of SL2 and cSL2 sequences, we found that the nature of the nucleotide backbone marginally influences the kinetics and mechanism of the peptide E-promoted annealing reaction. This is again in sharp contrast to HIV-1 NCp7, where major differences have been observed between the RNA and DNA sequences (31), as a result of different binding modes of NCp7 to the DNA and RNA sugars (52,53). These different modes appear as a consequence of the strong contacts of the sugars with the hydrophobic platform at the surface of the folded finger motifs. Both the absence of folded structures in the core peptide and the marginal differences between the core-promoted annealing of DNA and RNA sequences suggest that contacts between the core and the sugars in the ODNs are marginal, further underlining that electrostatic interactions between the basic residues and the negatively charged phosphate groups are the driving forces for the peptide E-promoted annealing reactions. These findings could also explain the lack of specific core-binding site on HCV genomic RNA, which is again in contrast to the presence of high affinity binding sites on the viral RNA genome, in case of HIV-1 NCp7 (53). The major role of electrostatic interactions in the core chaperone properties was further substantiated by the differences between peptides E, F and the D1 domain in their efficiency to promote the annealing of complementary sequences, which parallels the peptide charge number and density.

In conclusion, our data on the HCV RNA sequences further show that the core protein exhibits potent *in vitro* nucleic acid chaperone activities, facilitating RNA–RNA and RNA–DNA interactions and structural rearrangements (19,26,27). These chaperone activities seem to largely result from non-specific electrostatic interactions of the D1 domain with the phosphate groups of the RNA backbone. This is in sharp contrast with the chaperone properties of the NCp7 protein of HIV-1, which largely rely on the binding of NCp7 to specific binding sites on the viral RNA or DNA (44,52). Nevertheless, though the HIV-1 NCp7 and HCV core proteins exhibit different binding specificities for their nucleic acid targets, they are both able to promote annealing pathways that are absent or minor in their absence. Through its ability to promote the annealing of multiple sequences through various pathways, the core may contribute to the genetic variability of HCV by enhancing the frequency of copy-choice recombination (54,55) as it has been shown for NCp7 in the case of HIV-1 (47,56). Moreover, since the HCV genomic RNA adopts different conformations during the viral life cycle, we can speculate that the core protein can promote the interconversion between these different structures, and thus regulate the transitions between translation and replication as well as between replication and packaging of the genomic RNA.

SUPPLEMENTARY DATA

Supplementary Data are available at NAR Online: Supplementary Table 1 and Supplementary Figures 1 and 2.

ACKNOWLEDGEMENTS

We acknowledge Ludovic Richert for his help in performing time-resolved experiments.

FUNDING

Agence Nationale de Recherche sur le SIDA and FINOVI (Lyon, France). Funding for open access charge: Agence Nationale de Recherches sur le Sida.

Conflict of interest statement. None declared.

REFERENCES

1. Giannini,C. and Brechot,C. (2003) Hepatitis C virus biology. *Cell Death Differ*., **10(Suppl 1)**, S27–38.
2. Ghany,M.G., Strader,D.B., Thomas,D.L. and Seeff,L.B. (2009) Diagnosis, management, and treatment of hepatitis C: an update. *Hepatology*, **49**, 1335–1374.
3. Blight,K.J., Kolykhalov,A.A. and Rice,C.M. (2000) Efficient initiation of HCV RNA replication in cell culture. *Science*, **290**, 1972–1974.
4. Moradpour,D., Penin,F. and Rice,C.M. (2007) Replication of hepatitis C virus. *Nat. Rev. Microbiol*., **5**, 453–463.
5. Penin,F., Dubuisson,J., Rey,F.A., Moradpour,D. and Pawlotsky,J.M. (2004) Structural biology of hepatitis C virus. *Hepatology*, **39**, 5–19.
6. Bartenschlager,R., Penin,F., Lohmann,V. and Andre,P. (2011) Assembly of infectious hepatitis C virus particles. *Trends Microbiol*., **19**, 95–103.
7. Ito,T. and Lai,M.M. (1997) Determination of the secondary structure of and cellular protein binding to the 3′-untranslated region of the hepatitis C virus RNA genome. *J. Virol*., **71**, 8698–8706.
8. Song,Y., Friebe,P., Tzima,E., Junemann,C., Bartenschlager,R. and Niepmann,M. (2006) The hepatitis C virus RNA 3′-untranslated region strongly enhances translation directed by the internal ribosome entry site. *J. Virol*., **80**, 11579–11588.
9. Friebe,P., Boudet,J., Simorre,J.P. and Bartenschlager,R. (2005) Kissing-loop interaction in the 3′ end of the hepatitis C virus genome essential for RNA replication. *J. Virol*., **79**, 380–392.
10. Tsukiyama-Kohara,K., Iizuka,N., Kohara,M. and Nomoto,A. (1992) Internal ribosome entry site within hepatitis C virus RNA. *J. Virol*., **66**, 1476–1483.

11. Wang,C., Sarnow,P. and Siddiqui,A. (1993) Translation of human hepatitis C virus RNA in cultured cells is mediated by an internal ribosome-binding mechanism. *J. Virol.*, **67**, 3338–3344.
12. Blight,K.J. and Rice,C.M. (1997) Secondary structure determination of the conserved 98-base sequence at the 3′ terminus of hepatitis C virus genome RNA. *J. Virol.*, **71**, 7345–7352.
13. Kolykhalov,A.A., Feinstone,S.M. and Rice,C.M. (1996) Identification of a highly conserved sequence element at the 3′ terminus of hepatitis C virus genome RNA. *J. Virol.*, **70**, 3363–3371.
14. Friebe,P. and Bartenschlager,R. (2002) Genetic analysis of sequences in the 3′ nontranslated region of hepatitis C virus that are important for RNA replication. *J. Virol.*, **76**, 5326–5338.
15. Kolykhalov,A.A., Mihalik,K., Feinstone,S.M. and Rice,C.M. (2000) Hepatitis C virus-encoded enzymatic activities and conserved RNA elements in the 3′ nontranslated region are essential for virus replication in vivo. *J. Virol.*, **74**, 2046–2051.
16. Yanagi,M., St Claire,M., Emerson,S.U., Purcell,R.H. and Bukh,J. (1999) In vivo analysis of the 3′ untranslated region of the hepatitis C virus after in vitro mutagenesis of an infectious cDNA clone. *Proc. Natl Acad. Sci. USA*, **96**, 2291–2295.
17. Yi,M. and Lemon,S.M. (2003) 3′ nontranslated RNA signals required for replication of hepatitis C virus RNA. *J. Virol.*, **77**, 3557–3568.
18. Yi,M. and Lemon,S.M. (2003) Structure-function analysis of the 3′ stem-loop of hepatitis C virus genomic RNA and its role in viral RNA replication. *RNA*, **9**, 331–345.
19. Ivanyi-Nagy,R., Kanevsky,I., Gabus,C., Lavergne,J.P., Ficheux,D., Penin,F., Fosse,P. and Darlix,J.L. (2006) Analysis of hepatitis C virus RNA dimerization and core-RNA interactions. *Nucleic Acids Res.*, **34**, 2618–2633.
20. Shetty,S., Kim,S., Shimakami,T., Lemon,S.M. and Mihailescu,M.R. (2010) Hepatitis C virus genomic RNA dimerization is mediated via a kissing complex intermediate. *RNA*, **16**, 913–925.
21. Baumert,T.F., Ito,S., Wong,D.T. and Liang,T.J. (1998) Hepatitis C virus structural proteins assemble into viruslike particles in insect cells. *J. Virol.*, **72**, 3827–3836.
22. Kunkel,M., Lorinczi,M., Rijnbrand,R., Lemon,S.M. and Watowich,S.J. (2001) Self-assembly of nucleocapsid-like particles from recombinant hepatitis C virus core protein. *J. Virol.*, **75**, 2119–2129.
23. Shimoike,T., Mimori,S., Tani,H., Matsuura,Y. and Miyamura,T. (1999) Interaction of hepatitis C virus core protein with viral sense RNA and suppression of its translation. *J. Virol.*, **73**, 9718–9725.
24. Boulant,S., Montserret,R., Hope,R.G., Ratinier,M., Targett-Adams,P., Lavergne,J.P., Penin,F. and McLauchlan,J. (2006) Structural determinants that target the hepatitis C virus core protein to lipid droplets. *J. Biol. Chem.*, **281**, 22236–22247.
25. Boulant,S., Vanbelle,C., Ebel,C., Penin,F. and Lavergne,J.P. (2005) Hepatitis C virus core protein is a dimeric alpha-helical protein exhibiting membrane protein features. *J. Virol.*, **79**, 11353–11365.
26. Cristofari,G., Ivanyi-Nagy,R., Gabus,C., Boulant,S., Lavergne,J.P., Penin,F. and Darlix,J.L. (2004) The hepatitis C virus Core protein is a potent nucleic acid chaperone that directs dimerization of the viral (+) strand RNA in vitro. *Nucleic Acids Res.*, **32**, 2623–2631.
27. Sharma,K., Didier,P., Darlix,J.L., de Rocquigny,H., Bensikaddour,H., Lavergne,J.P., Penin,F., Lessinger,J.M. and Mely,Y. (2010) Kinetic analysis of the nucleic acid chaperone activity of the hepatitis C virus core protein. *Nucleic Acids Res.*, **38**, 3632–3642.
28. Bernacchi,S., Stoylov,S., Piemont,E., Ficheux,D., Roques,B.P., Darlix,J.L. and Mely,Y. (2002) HIV-1 nucleocapsid protein activates transient melting of least stable parts of the secondary structure of TAR and its complementary sequence. *J. Mol. Biol.*, **317**, 385–399.
29. Egele,C., Piemont,E., Didier,P., Ficheux,D., Roques,B., Darlix,J.L., de Rocquigny,H. and Mely,Y. (2007) The single-finger nucleocapsid protein of moloney murine leukemia virus binds and destabilizes the TAR sequences of HIV-1 but does not promote efficiently their annealing. *Biochemistry*, **46**, 14650–14662.
30. Egele,C., Schaub,E., Piemont,E., de Rocquigny,H. and Mely,Y. (2005) Investigation by fluorescence correlation spectroscopy of the chaperoning interactions of HIV-1 nucleocapsid protein with the viral DNA initiation sequences. *C. R. Biol.*, **328**, 1041–1051.
31. Godet,J., de Rocquigny,H., Raja,C., Glasser,N., Ficheux,D., Darlix,J.L. and Mely,Y. (2006) During the early phase of HIV-1 DNA synthesis, nucleocapsid protein directs hybridization of the TAR complementary sequences via the ends of their double-stranded stem. *J. Mol. Biol.*, **356**, 1180–1192.
32. Ramalanjaona,N., de Rocquigny,H., Millet,A., Ficheux,D., Darlix,J.L. and Mely,Y. (2007) Investigating the mechanism of the nucleocapsid protein chaperoning of the second strand transfer during HIV-1 DNA synthesis. *J. Mol. Biol.*, **374**, 1041–1053.
33. Vo,M.N., Barany,G., Rouzina,I. and Musier-Forsyth,K. (2009) HIV-1 nucleocapsid protein switches the pathway of transactivation response element RNA/DNA annealing from loop-loop "kissing" to "zipper". *J. Mol. Biol.*, **386**, 789–801.
34. Cristofari,G. and Darlix,J.L. (2002) The ubiquitous nature of RNA chaperone proteins. *Prog. Nucleic Acid Res. Mol. Biol.*, **72**, 223–268.
35. Herschlag,D. (1995) RNA chaperones and the RNA folding problem. *J. Biol. Chem.*, **270**, 20871–20874.
36. Ward,D.C., Reich,E. and Stryer,L. (1969) Fluorescence studies of nucleotides and polynucleotides. I. Formycin, 2-aminopurine riboside, 2,6-diaminopurine riboside, and their derivatives. *J. Biol. Chem.*, **244**, 1228–1237.
37. Bloomfield,V.A., He,S., Li,A.Z. and Arscott,P.B. (1991) Light scattering studies on DNA condensation. *Biochem. Soc. Trans.*, **19**, 496.
38. Hargittai,M.R., Gorelick,R.J., Rouzina,I. and Musier-Forsyth,K. (2004) Mechanistic insights into the kinetics of HIV-1 nucleocapsid protein-facilitated tRNA annealing to the primer binding site. *J. Mol. Biol.*, **337**, 951–968.
39. Kuzmic,P. (1996) Program DYNAFIT for the analysis of enzyme kinetic data: application to HIV proteinase. *Anal. Biochem.*, **237**, 260–273.
40. Cantor,C. and Schimmel,P. (1980) *Biophysical Chemistry Part 2: Techniques for the Study of Biological Structure and Function*. Academic Press, New York, USA.
41. Rouzina,I. and Bloomfield,V.A. (1999) Heat capacity effects on the melting of DNA. 1. General aspects. *Biophys. J.*, **77**, 3242–3251.
42. Avilov,S.V., Piemont,E., Shvadchak,V., de Rocquigny,H. and Mely,Y. (2008) Probing dynamics of HIV-1 nucleocapsid protein/target hexanucleotide complexes by 2-aminopurine. *Nucleic Acids Res.*, **36**, 885–896.
43. Jean,J.M. and Hall,K.B. (2001) 2-Aminopurine fluorescence quenching and lifetimes: role of base stacking. *Proc. Natl Acad. Sci. USA*, **98**, 37–41.
44. Guest,C.R., Hochstrasser,R.A., Sowers,L.C. and Millar,D.P. (1991) Dynamics of mismatched base pairs in DNA. *Biochemistry*, **30**, 3271–3279.
45. Godet,J., Ramalanjaona,N., Sharma,K.K., Richert,L., de Rocquigny,H., Darlix,J.L., Duportail,G. and Mely,Y. (2011) Specific implications of the HIV-1 nucleocapsid zinc fingers in the annealing of the primer binding site complementary sequences during the obligatory plus strand transfer. *Nucleic Acids Res.*, **39**, 6633–6645.
46. Ivanyi-Nagy,R., Davidovic,L., Khandjian,E.W. and Darlix,J.L. (2005) Disordered RNA chaperone proteins: from functions to disease. *Cell. Mol. Life Sci.*, **62**, 1409–1417.
47. Rein,A., Henderson,L.E. and Levin,J.G. (1998) Nucleic-acid-chaperone activity of retroviral nucleocapsid proteins: significance for viral replication. *Trends Biochem. Sci.*, **23**, 297–301.
48. Azoulay,J., Clamme,J.P., Darlix,J.L., Roques,B.P. and Mely,Y. (2003) Destabilization of the HIV-1 complementary sequence of TAR by the nucleocapsid protein through activation of conformational fluctuations. *J. Mol. Biol.*, **326**, 691–700.
49. Cosa,G., Zeng,Y., Liu,H.W., Landes,C.F., Makarov,D.E., Musier-Forsyth,K. and Barbara,P.F. (2006) Evidence for

non-two-state kinetics in the nucleocapsid protein chaperoned opening of DNA hairpins. *J. Phys. Chem. B*, **110**, 2419–2426.
50. Tompa,P. and Csermely,P. (2004) The role of structural disorder in the function of RNA and protein chaperones. *FASEB J.*, **18**, 1169–1175.
51. Godet,J. and Mely,Y. (2010) Biophysical studies of the nucleic acid chaperone properties of the HIV-1 nucleocapsid protein. *RNA Biol.*, **7**, 48–60.
52. Bazzi,A., Zargarian,L., Chaminade,F., Boudier,C., De Rocquigny,H., Rene,B., Mely,Y., Fosse,P. and Mauffret,O. (2011) Structural insights into the cTAR DNA recognition by the HIV-1 nucleocapsid protein: role of sugar deoxyriboses in the binding polarity of NC. *Nucleic Acids Res.*, **39**, 3903–3916.
53. Darlix,J.L., Godet,J., Ivanyi-Nagy,R., Fosse,P., Mauffret,O. and Mely,Y. (2011) Flexible nature and specific functions of the HIV-1 nucleocapsid protein. *J. Mol. Biol.*, **410**, 565–581.
54. Kalinina,O., Norder,H., Mukomolov,S. and Magnius,L.O. (2002) A natural intergenotypic recombinant of hepatitis C virus identified in St. Petersburg. *J. Virol.*, **76**, 4034–4043.
55. Yokoyama,K., Takahashi,M., Nishizawa,T., Nagashima,S., Jirintai,S., Yotsumoto,S., Okamoto,H. and Momoi,M.Y. (2011) Identification and characterization of a natural inter-genotypic (2b/1b) recombinant hepatitis C virus in Japan. *Arch. Virol.*, **156**, 1591–1601.
56. Darlix,J.L., Garrido,J.L., Morellet,N., Mely,Y. and de Rocquigny,H. (2007) Properties, functions, and drug targeting of the multifunctional nucleocapsid protein of the human immunodeficiency virus. *Adv. Pharmacol.*, **55**, 299–346.